Applied Surface Science 562 (2021) 150019

Contents lists available at ScienceDirect

Applied Surface Science

journal homepage: www.elsevier.com/locate/apsusc

Full Length Article

Hydrogen storage capacity of Li-decorated borophene and pristine graphene slit pores: A combined ab initio and quantum-thermodynamic study

I. Cabria [a,*], A. Lebon [b], M.B. Torres [c], L.J. Gallego [d], A. Vega [a]

[a] Departamento de Física Teórica, Atómica y Óptica, Universidad de Valladolid, ES-47011 Valladolid, Spain
[b] Laboratoire de Chimie Electrochimie Moléculaire et Chimie Analytique, Université de Brest, UMR CNRS 6521, F-29285 Brest, France
[c] Departamento de Matemáticas y Computación, Escuela Politécnica Superior, Universidad de Burgos, ES-09006 Burgos, Spain
[d] Departamento de Física de la Materia Condensada, Facultad de Física, Universidad de Santiago de Compostela, ES-15782 Santiago de Compostela, Spain

ARTICLE INFO

Keywords:
Hydrogen storage
2D materials
Boron-based materials
Li-decorated materials
Statistical physics

ABSTRACT

Among the two-dimensional materials of the post-graphene era, borophene has raised an enormous interest due to its unprecedented diversity of structures and the wide variety of potential applications, including its ability for hydrogen storage. In the present paper we use van der Waals-corrected density functional theory in conjunction with a quantum-thermodynamic model to investigate the hydrogen storage capacity of confining Li-decorated borophene sheets in its most stable Pmmn8 configuration. Our theoretical approach surpasses the standard density functional theory calculations only valid at zero temperature and no pressure, thus providing the gravimetric and volumetric capacities as well as the isotherms in real conditions. We show that narrow Li-decorated slit pores of borophene have a good volumetric hydrogen storage capacity particularly at low temperature. Accordingly, nanoporous boron frameworks could be optimal for hydrogen storage in applications at low temperature. We compare the results with those corresponding to pristine graphene slit pores.

1. Introduction

Although the current fleet of hydrogen-powered vehicles is still very limited, they are considered the next-generation of electric vehicles and firm candidates to replace the conventional fossil fuel vehicles in the coming years or, at least, be an efficient alternative within a world of presumable multiple solutions to meet the energy, the pollution and the climate challenges. So far, only some companies offer models, but quite expensive, and others are currently working in hydrogen car projects. Hydrogen is abundant and cheap and its combustion produces three times as much energy as an equivalent quantity of petrol; moreover, the result of this combustion is clean water (i.e., no CO_2 and no other harmful gases are produced), so that it is environmentally benign. Despite its advantages, the use of hydrogen involves technical challenges and rise questions about efficiency. Hydrogen extraction in the most efficient way requires a chemical process, such as water-splitting electrolysis or the reaction of hydrocarbon chains at high temperature. Although there exist non-chemical ways to produce hydrogen, like by means of algae and solar light [1–3], they are very slow, compared with the chemical processes. Anyway, the hydrogen storage still remains a most critical problem [4–11].

Currently, hydrogen is stored in high-pressure tanks or in its liquid state at cryogenic facilities. Both ways present risks and inconveniences, which has made necessary the search for alternative methods of storage. Adsorption on light materials with large surface/volume ratio is being considered as the next step for hydrogen storage. Within this context, carbon-based nanostructures such as graphene or carbon nanotubes have emerged as the most promising alternative due to their remarkable thermal and mechanical properties (see, e.g., Refs. [12–14] and those cited therein). To be used in hydrogen-powered vehicles, a material requires a gravimetric storage capacity of 4.5 wt% and a volumetric storage capacity of 0.030 kg/L of H_2 at room temperature and moderate pressure, as established by the U.S. Department of Energy (DOE) [15,16].

To achieve reversible storage of H_2 at room temperature and moderate pressure, the binding energy needs to be 0.1–0.3 eV per molecule (i.e., in a range between physisorption and chemisorption), as has been shown for a number of surfaces [17,18]. Low-dimensional carbon

* Corresponding author.
E-mail address: ivan.cabria@uva.es (I. Cabria).

https://doi.org/10.1016/j.apsusc.2021.150019
Received 13 November 2020; Received in revised form 5 April 2021; Accepted 1 May 2021
Available online 19 May 2021

nanotubes and graphene-based systems do not meet such H_2-binding energy requirement. However, it has been found that doping or decoration (since these are non bulk-like structures) with carefully selected species can substantially increase their hydrogen storage ability. A pioneering work in this area was performed by Yildirim and Ciraci [19], who used density functional theory (DFT) to show that Ti-decorated single-walled carbon nanotubes are promising candidates for high-capacity hydrogen storage media. A similar conclusion was also obtained by Lebon et al. [20] for Ti-decorated zigzag graphene nanoribbons.

Cabria et al. [21,22] applied a quantum-thermodynamic model to calculate the storage capacities of nanoporous carbons in a range of pressures and temperatures as a function of the size and shape of the carbon pores. The model, which is an improvement of the model proposed by Patchkovskii et al. [23], takes into account the quantum effects of the motion of H_2 in the confining potential of the pores. The storage capacities calculated at room temperature are far too short to reach the DOE capacity targets. The reason is that, in spite of the confinement effect, which can be varied by modification of the pore shape and size, the interaction between H_2 and the carbon surfaces is not attractive enough.

Concurrently with the research on carbon-based nanostructures, there has been a growing interest in recent years in two-dimensional (2D) materials beyond graphene (see, e.g., Refs. [24–28]). Theoretical studies seem to indicate that hundreds of 2D novel compounds should exist, which have since led to the successful synthesis and characterization of many of them. As one can easily imagine, 2D materials display a large diversity of chemical, mechanical, electronic and optical properties and a wide range of potential applications, such as nanoelectronics, spintronics, optoelectronics or even in nanomedicine. Furthermore, some of those novel 2D materials have been proposed as electrodes in novel batteries or as novel hydrogen storage solid state devices. Among the large family of novel 2D compounds, borophene has attracted a great interest because of its intriguing and diverse properties, which arise from a large variety of geometrical structures and bonding patterns. Borophene has also been proposed as a suitable material for a wide range of applications, including metal-ion batteries, supercapacitors, sensors, catalytic devices, and others in medicine, to say the least (see a recent review in Ref. [29]).

We note that although the existence of the boron counterpart of graphene was theoretically predicted some years ago, it was not synthesized until recently using Ag(111) as underlying substrate [30]. DFT predictions for the structure of borophene went from initial single-atomic layers made of triangular and hexagonal arrangements, the so-called α-sheet [31], to novel nonplanar phases that are thermodynamically more favorable [32]. One of such phases displays a complex buckled geometry with Pmmn symmetry and eight atoms in the unit cell. In this work we will refer to it as the Pmmn8 phase or the β-sheet. The boron monolayer synthesized on Ag(111) [30] shows the same Pmmn symmetry, but first-principles relaxation of such a monolayer results in loss of corrugation along one of the in-plane directions, while keeping the buckled structure along the other [30]. The resulting free standing borophene has only two atoms per unit cell. We will denote it as Pmmn2 or simply the γ-sheet. Phonon spectra calculations [33,34], by forcing translational symmetry and rotational symmetry, reveal that the most stable phase of borophene is the β-sheet.

The three phases of borophene indicated above have been investigated as candidates for hydrogen storage. DFT-GGA calculations show that the Li-decorated α-sheet can contain up to 10.7 wt% of molecular hydrogen [35], with an average binding energy of 0.15 eV, which exceeds the capacity of the graphene-based counterpart. Moreover, the Li-decorated γ-sheet can reach a capacity of 13.7 wt% and H_2-binding energies that also satisfy the binding energy requirement, as obtained using GGA-DFT and van der Waals (vdW)-corrected DFT calculations [36]. Recently, Lebon et al. [37] investigated the Li-decorated β-sheet, using the non-local optB88-vdW functional proposed by Klimeš et al. [38]. Satisfactory H_2-binding energies were reported, but the obtained gravimetric density was 3.84 wt %, slightly lower than the 4.5 wt % DOE threshold. However, all these results must be taken cautiously as they correspond to ground state calculations at $T = 0$ K; in other words, finite temperature and pressure are not accounted for.

In order to get a more realistic information on the hydrogen storage capacity of borophene, in the work described here we use the quantum-thermodynamic model of Cabria et al. [21,22] to investigate the temperature and pressure-dependencies of the gravimetric and volumetric hydrogen storage capacities of borophene nanostructures under doping and extreme conditions of confinement. Specifically, we considered a slit pore consisting of two parallel Li-decorated Pmmn8 borophene sheets (i.e., in the most stable configuration of borophene), separated by a certain distance, with hydrogen molecules in between. Hence, our aim goes beyond the standard ($T = 0$ K) DFT calculations in this field. We note that the system considered in this paper is much more complex than that studied by Cabria et al. [21,22], not only for the complexity of the Pmmn8 structure of the borophene walls, but also for the fact that it is not in pristine form, but doped with Li atoms. We also note that nanoporous boron frameworks, containing many regions of borophene slit-shaped pores, could perhaps be formed by using zeolite as a sacrificial template, just as zeolite-template carbons (ZTC) are formed [39].

The following sections of this paper are organized as follows. In Section 2 we give the essential technical details of the computational method used, the geometry of the slit pore of Li-decorated β borophene sheets and of the general features of the quantum-thermodynamic model employed to obtain the temperature and pressure dependent figures of merit. In Section 3 we present and discuss our results for the gravimetric and volumetric hydrogen storage capacities of these nanostructures, compare them with the results obtained for graphene slit pores, and explain our findings in the light of the interaction potentials confining the hydrogen molecule in the slit pores. Finally, in Section 4, we summarize our main conclusions.

2. Research methodology

2.1. Computational method

The quantum-thermodynamic model employed in this work (briefly outlined in a subsection below) accounts for quantum-confinement effects due to the nanometric dimensions of the pores in which the H_2 molecules are stored. These effects lead to the quantization of the energy spectrum of the molecule within the interaction potential of the slit pore. Those energy states are required in the quantum-thermodynamic model and, therefore, solving the Schrödinger equation for the Hamiltonian of the H_2 molecule in the interaction potential of the slit pore is the first step. Previously, we had to accurately determine the three-dimensional interaction potential of H_2 in the slit pore. This was accomplished by performing calculations within the DFT as implemented in the VASP package [40,41]. This package solves the Kohn-Sham equations within the projector-augmented wave (PAW) approach [42]. For the plane-wave basis, a cut-off energy of 500 eV was used. In the calculations we employed the non-local optB88-vdW functional of Klimeš et al. [38], which includes the dispersion interactions. A k-point space of about 0.2 $Å^{-1}$ was used for integrating Brillouin zones. The width of the Gaussian smearing used was 0.01 eV. The interactions between periodic images of the sheet along the normal to the surface are negligible, because they were separated by a distance of 23 Å.

As in Ref. [37], we used a 2×2 supercell of the β borophene sheet made of 32 B atoms. The sheet was decorated with 4 Li atoms on both sides, and the resulting hybrid nanostructure was relaxed using the conjugated-gradient method until the total force on each atom was smaller than 0.01 eV/Å; the accuracy to convergence for the total energies was 10^{-6} eV/unit cell. The dependency of the stability of Li-decorated borophene with Li concentration was extensively studied by some of us in the previous work [37]. In the present study we shall

consider the Li-decorated borophene sheet with its most stable Li concentration. The relaxed structure of the Li-decorated β sheet is schematically represented in Fig. 1, which shows that the preferential adsorption sites of the Li atoms on the β sheet are the furrow sites. The same figure also shows the location of an H_2 molecule adsorbed on the Li-decorated β sheet in its most stable configuration.

The interaction potential energy, $V(x,y,z)$, of a hydrogen molecule located at point (x,y,z) with the Li-decorated β borophene sheet is defined as

$$V(x,y,z) = E(H_2@Li\text{-}borophene) - E(H_2) - E(Li\text{-}borophene), \quad (1)$$

where $E(H_2@Li\text{-}borophene), E(H_2)$ and $E(Li\text{-}borophene)$ are the energy of H_2 at (x,y,z) on the Li-decorated β borophene sheet, the energy of an isolated H_2 molecule and the energy of the Li-decorated β borophene sheet, respectively, and z is the distance between the H_2 molecule and the sheet surface.

We calculated the physisorption energies (or $V(x,y,z)$) of a single H_2 molecule (with the most stable orientation) on the surface of the relaxed Li-decorated β borophene sheet using the optB88-vdW functional [38]. Thus we obtained the interaction potential energy between the H_2 molecule and the Li-decorated borophene sheet, $V(x,y,z)$. In our calculations we chose a xy grid with $\Delta x = \Delta y = 0.25$ Å. This implies 936 grid points in the xy-plane. Then, for each one of these xy points or regions, we placed the H_2 molecule at different values of z, ranging from 0.8 to 7.6 Å, near to the surface of the sheet, with a step between points $\Delta z = 0.125$ Å. Then, we made calculations for each one of these (x,y,z) grid points, and consequently we obtained a numerical three-dimensional $V(x,y,z)$ interaction potential.

A slice of the three-dimensional interaction potential energy $V(x,y,z)$ is plotted in left and middle panels of Fig. 2. It corresponds to the interaction potential energy in two planes, $z = 2.58$ and 3.33 Å. It can be noticed that the deepest regions correspond to the neighbourhood of the Li atoms. In right panel of Fig. 2, the potential is shown for two constant pairs of (x,y) grid points, those where the resulting curves $V(z)$ are the deepest and the shallowest ones among the 936 $V(z)$ curves obtained in the calculations. The latter figure also contains the interaction potential $V(z)$ between a H_2 molecule and a graphene layer in the isotropic approximation mentioned later, as obtained using the optB88-vdW functional.

2.2. Geometry of the slit pores formed by two parallel Li-decorated borophene sheets

We have used the geometry of the Li-decorated β borophene sheet to build slit-shaped pores. According to experiments [43], nanoporous carbons contain many regions that are flat, graphitic-like parallel surfaces separated by a distance of some nanometers. Those regions are called slit pores. Graphene slit pores were studied in Ref. [44] using the optB88-vdW functional, with the isotropic approximation for the interaction potential of H_2 with graphene. The volumetric capacities, v_c, of graphene slit pores published in Ref. [44] will be plotted in this work for comparative purposes. Other results presented here for graphene slit pores (the gravimetric capacities, g_c, and the interaction potentials) are entirely new, although related with the results reported in that reference. The upper panel of Fig. 3 shows the model of the slit borophene pore used in our investigation of the hydrogen storage capacity of these nanostructures, consisting in two parallel Li-decorated β borophene sheets separated by a distance d. The interactions between the H_2 molecule and the graphene and Li-decorated borophene slit pores are due to dispersion forces. These interactions are very weak, so that the adsorption and desorption of the H_2 molecules at 80.15 and 298.15 K (the two temperatures considered in this work) do not destabilize the structure of these pores.

2.3. Quantum-thermodynamic model

The quantum-thermodynamic model has been explained in detail in Refs. [21,22,44]. The model is based on considering the thermodynamic equilibrium between the adsorbed and compressed phases of hydrogen gas inside a slit pore. These phases have been drawn schematically in Fig. 3 (lower panel). The H_2 molecules stored by physisorption on the pore surface form the adsorbed phase (the blue and purple regions in the lower panel of Fig. 3) and the H_2 molecules stored only by compression, without interacting with the pore surface, form the compressed phase (the region with red balls in the lower panel of Fig. 3).

The model uses the interaction potential energy $V(x,y,z)$ of one single layer (Li-decorated borophene, graphene, etc.), where z is the distance to the layer surface. The interaction potential energy of a slit pore of width d, or slit pore potential, is the sum of the potentials of the corresponding two parallel layers: $V_{slitpore}(z;d) = V(x,y,z) + V(x,y,d-z)$. The slit pore is confined in the z direction. The sheets or layers of the slit pore are located at $z = 0$ and $z = d$.

In the case of a graphene slit pore, the potential energy of one single layer depends very little on the sites (x,y), and hence the approximations $V(x,y,z) = V(z)$ for a single layer and $V(z) + V(d-z)$ for a slit pore are sound approximations. As regards to the Li-decorated borophene slit pore, the potential energy of a single layer has a strong dependence on the sites (x,y). Therefore, we have used three-dimensional potentials for a Li-decorated borophene single layer, $V(x,y,z)$, and for a Li-decorated borophene slit pore, $V(x,y,z) + V(x,y,d-z)$.

The equation of the equilibrium between the two phases inside a pore is, in the quantum-thermodynamic model,

$$ln(Z_{ads}/Z_{com}) = \frac{1}{RT}\int_{P_{com}}^{P_{ads}} v_{mol}(P,T)dP, \quad (2)$$

where Z_{ads} and Z_{com} are the partition functions of the adsorbed and

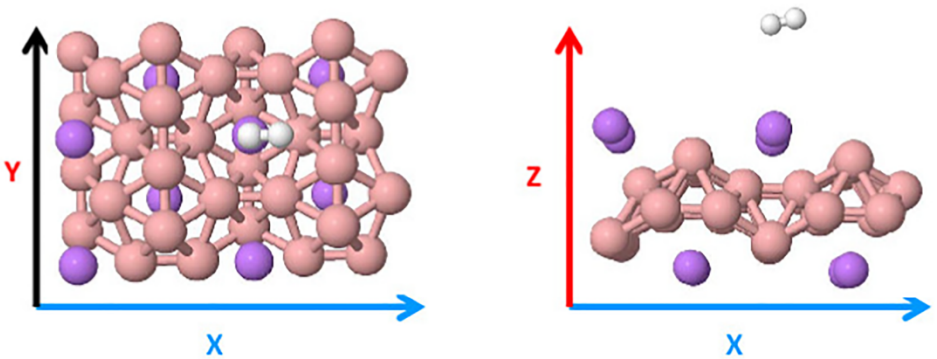

Fig. 1. Front and side views of the relaxed 2 × 2 supercell of the β (Pmmn8) sheet decorated with 4 Li atoms at furrow sites on each side of the sheet. Li atoms are shown with purple balls. Also shown is an adsorbed H_2 molecule in its most stable configuration (with H atoms in white).

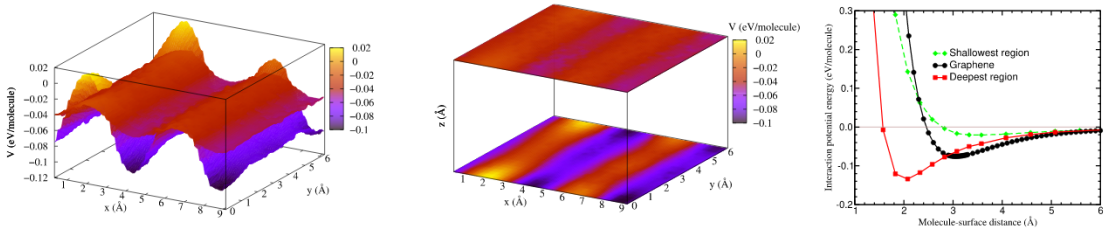

Fig. 2. Interaction potential energy between a single Li-decorated β borophene sheet and a H_2 molecule in the planes z = 2.58 and 3.33 Å plotted in 3D (left panel) and its projections in the xy plane (middle panel). The bottom and upper 3D surfaces (planes) of the left (middle) panel correspond to the planes z = 2.58 and 3.33 Å, respectively. Right panel: Interaction potential energy between a H_2 molecule and a single graphene layer, and a single Li-decorated β borophene sheet at the deepest and shallowest *xy* points, as a function of the H_2 molecule-surface distance.

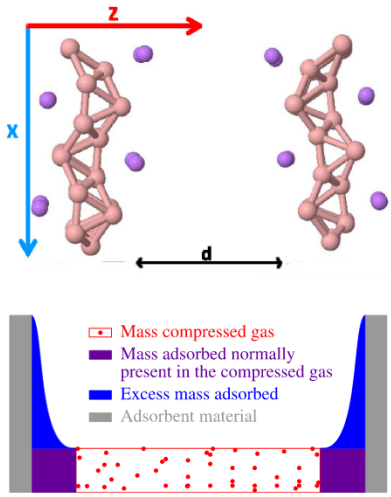

Fig. 3. Upper panel: Geometrical structure of a Li-decorated borophene slit pore of width *d*, made of two parallel Li-decorated β borophene sheets. Lower panel: Schematic representation of the phases of hydrogen stored inside a slit pore.

compressed hydrogen phases, respectively, P_{com} and P_{ads} are the pressures of the adsorbed and compressed phases, respectively, and $v_{\mathrm{mol}}(P, T)$ is the molar volume of hydrogen. The partition functions are given by

$$Z_{\mathrm{ads}} = \sum e^{-\epsilon_i/k_B T}, \tag{3}$$

$$Z_{\mathrm{com}} = (d - 2d_{\mathrm{excl}})\sqrt{2\pi m k_B T/h^2}. \tag{4}$$

In those equations, k_B is the Boltzmann constant, ϵ_i are the eigenenergies of the quantum states of a single H_2 molecule in the slit pore potential $V_{slitpore}(z; d)$, obtained by solving the corresponding Schrödinger equation, *m* is the mass of a hydrogen molecule, *h* is the Planck's constant, *d* is the slit pore width and d_{excl} is an exclusion distance due to the repulsive region of the interaction potential energy of a single layer. The repulsive region is the region close to the atoms that form the layer.

The exclusion distance is defined as the location where the repulsive region of the interaction potential energy of a single layer is 1 eV. If the interaction potential energy of a single layer depends on (x, y, z), then there is an exclusion distance for each site (x, y) and the model uses the average exclusion distance. If the interaction potential energy of a single layer depends only on *z*, then the exclusion distance is that of the $V(z)$ potential energy.

The mass of hydrogen stored in the pore is the sum of the masses of the adsorbed and compressed hydrogen. In this investigation, we will calculate and compare only the storage capacities due to the adsorbed phase, because the differences between the hydrogen storage capacities of Li-decorated β borophene and graphene slit pores come from the different interaction with the pore surfaces, which impacts only on the adsorbed phase. The gravimetric capacity, g_c, of Li-decorated β borophene and graphene slit pores are also different because of the different masses of the adsorbent sheets of the pores.

The quantum-thermodynamic model calculates the molar volume and the mass of the adsorbed phase and uses them to obtain the storage capacities. The model obtains the pressure of the adsorbed phase, P_{ads}, from the equation of the thermodynamic equilibrium between the two phases (Eq. 2). This pressure is used to calculate the molar volume of the adsorbed hydrogen phase, $v_{\mathrm{mol}}(P_{ads}, T)$, in L/mol. The molar volume of the adsorbed phase is that given by the Mills-Younglove equation of state of H_2 [22] at the pressure of the adsorbed phase: $v_{\mathrm{mol}}(P_{ads}, T) = v_{\mathrm{molMills-Younglove}}(P_{ads}, T)$. This molar volume will be used to calculate the volumetric and gravimetric capacities.

The volumetric capacity, v_c, of the adsorbed hydrogen phase is calculated, in kg of H_2/L, by means of the equation

$$v_c = \frac{M(H_2)}{v_{\mathrm{mol}}(P_{ads}, T)} \frac{V_{\mathrm{adsorbed}}}{V_{\mathrm{pore}}}, \tag{5}$$

where $M(H_2)$ is the molar mass of H_2 in kg/mol, 0.00201588 kg/mol, and V_{pore} and V_{adsorbed} are the volume of the pore and the volume of the adsorbed hydrogen phase, respectively.

An explanation of the calculation of the volume of the adsorbed phase, V_{adsorbed}, follows. First, it must be taken into account that the adsorbed phase inside a slit pore can be composed by one or two layers. In the lower panel of Fig. 3 the adsorbed hydrogen is the blue and violet regions. In that figure, there are two layers of adsorbed hydrogen. If the slit pore is narrow, then there is only one layer. If the slit pore is wide, then there are two layers and each layer is attached to one of the sheets of the slit pore.

The volume of the adsorbed phase is $V_{\mathrm{adsorbed}} = S w_{ads}$. The surface of one sheet is *S* and w_{ads} is the width of the adsorbed phase. If there is only one layer, then w_{ads} is the width of the layer. If there are two layers, then w_{ads} is the sum of the widths of the two layers. The width of the adsorbed phase is given by

$$w_{ads} = \begin{cases} z_r - z_l & z_r - z_l \leqslant 2L \\ 2L & z_r - z_l > 2L, \end{cases} \tag{6}$$

where z_r and z_l are the points at which $V_{slitpore}(z; d) = 0, z_r > z_l$ and *L* is the width of a layer adsorbed on a single and isolated sheet.

The value of *L* is 3 Å. This value was selected because is approximately the kinetic diameter of a H_2 molecule, 2.89 Å [45], the van der Waals diameter of a H_2 molecule, 2.76 Å [46], and also the equilibrium distance of most of the interaction potentials $V(z)$ of a physisorbed H_2 molecule on a single and isolated graphene and on other adsorbent surfaces.

To calculate g_c it is necessary to obtain the mass of the adsorbed phase, $mass_{Hadsorbed}$. This mass is obtained, in kg, as the product of the density in kg/L and the volume in liters of the adsorbed phase: $\rho_{\mathrm{adsorbed}} V_{\mathrm{adsorbed}}$. The density of the adsorbed phase is given by $a/v_{\mathrm{mol}}(P_{ads}, T)$. This amount was already used to calculate the volumetric capacity.

The g_c of the adsorbed hydrogen phase is calculated, in wt%, as

$$g_c = 100 \frac{mass_{Hadsorbed}}{mass_{Hadsorbed} + mass_{adsorbentmaterial}}, \quad (7)$$

where $mass_{adsorbentmaterial}$ is the mass of the adsorbent material of the slit-shaped pore. The concentration or coverage of hydrogen is defined in terms of volume (volumetric capacity measured in kg of H_2/L, Eq. 5) and relative weight (gravimetric capacity measured in relative weight, Eq. 7).

2.4. Interaction potential energy of the graphene slit pore

Although it is a huge computational task, a good sampling of the interaction potential energy landscape is crucial to accurately determine the adsorption capacities of the slit pore. We note that in previous works for graphene slit pores [21–23], only a one-dimensional potential, along the normal direction, $V(z)$, corresponding to the most stable physisorption site of H_2 on the surface, was calculated and assumed to be the same along the whole graphene unit cell, thus neglecting anisotropic effects; the hydrogen storage capacities were calculated according to that potential. This is a first approximation, but as we will see below, deep and shallow regions decorate the potential energy landscape, which means that results based on an isotropic potential in x,y, equal to that corresponding to the most stable configuration, slightly overestimate both the g_c and v_c. In other words, the confining potential used in previous works for carbon based slit pores is a bit more confining that the real one.

In our comparison of the hydrogen storage capacities of the Li-decorated borophene slit pores with those of graphene slit pores, we have used average capacities for the graphene slit pores. In a previous work on the hydrogen storage capacity of graphene slit pores [22], the H_2 adsorption energy was calculated for the nine main configurations of H_2 on graphene [47], and the reported capacity corresponded to the most stable configuration. A configuration is a combination of site and orientation of the molecule. The three main sites are on top of an hexagon (H), on top of a carbon atom (A) and on top of a C—C bond (B) (see Fig. 4). The three main orientations are perpendicular to the graphene surface ($\perp$), parallel to the graphene surface and parallel to two C—C bonds of a graphene hexagon ($\parallel\parallel$), and parallel to the graphene surface and perpendicular to two C—C bonds of a graphene hexagon ($\parallel\perp$). We obtained that the most stable configuration is $H_{\parallel\parallel}$.

In the present work, we have calculated the binding energy in more sites of graphene, with the H_2 molecule in the orientation $\parallel\parallel$. Specifically, in the sites A, B, H, AB, BH, AH and ABH indicated in Fig. 4 (site AB is located at the middle of the line joining sites A and B, and so on for the other new sites studied). The results are gathered in Table 1. The binding energies of H_2 on all the studied sites of graphene are very close, being the largest difference 0.0066 eV. The most stable site is H and the less stable site is A.

We have calculated the interaction potential energy $V(z)$ of H_2 on graphene for those two configurations, $H_{\parallel\parallel}$ and $A_{\parallel\parallel}$, and then we have used the potentials $V(z)$ and the quantum-thermodynamic model to calculate the corresponding storage capacities. The results are shown in

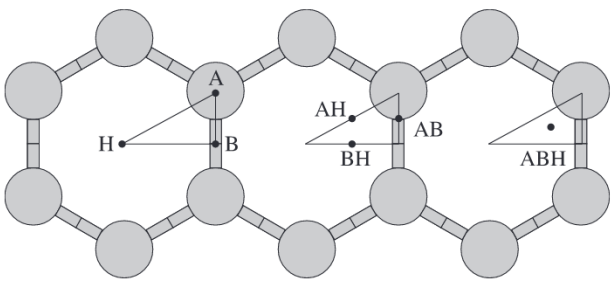

Fig. 4. Sites of H_2 on graphene.

Table 1
Binding energy of H_2 in eV, E_b, and equilibrium H_2-surface distance in Å, d_e, on different sites of graphene, as obtained by optB88-vdW calculations. The H_2 molecule is in the orientation $\parallel\parallel$.

Configuration	d_e	E_b	Configuration	d_e	E_b
$A_{\parallel\parallel}$	3.2	−0.0686	$AB_{\parallel\parallel}$	3.2	−0.0692
$B_{\parallel\parallel}$	3.2	−0.0696	$BH_{\parallel\parallel}$	3.1	−0.0723
$H_{\parallel\parallel}$	3.1	−0.0752	$AH_{\parallel\parallel}$	3.1	−0.0713
$ABH_{\parallel\parallel}$	3.2	−0.0704			

Fig. 5. The capacities with the H_2 molecule on the hexagon and on the carbon atom are very similar for large pore widths. The difference between the $H_{\parallel\parallel}$ and $A_{\parallel\parallel}$ capacities is larger at narrow pores. The capacities of the exact three-dimensional potential of a graphene slit pore should be between the $H_{\parallel\parallel}$ and $A_{\parallel\parallel}$ capacities. Hence, a sound approximation is to consider the capacities of the graphene slit pores as the average of the capacities obtained with the H_2 molecule on the configurations $H_{\parallel\parallel}$ and $A_{\parallel\parallel}$: $c = (c_{H_{\parallel\parallel}} + c_{A_{\parallel\parallel}})/2$. As indicated above, the capacities of graphene slit pores were computed in Ref. [22] using the most stable configuration, $H_{\parallel\parallel}$. However, the hydrogen storage capacities of graphene slit pores presented and discussed in the next section are precisely the average capacities deduced from the specific sites considered in Fig. 5.

3. Results and discussion

Using the quantum-thermodynamic model described above, we have investigated the hydrogen storage ability of slit pores of Li-decorated β borophene by performing extensive calculations of their g_c and v_c as functions of pore width, temperature and pressure. The storage capacities depend on the interaction potential $V(x,y,z)$ between the hydrogen molecules and the confining Li-decorated borophene sheets. The computed g_c and v_c of these slit pores will be compared with those obtained for graphene slit pores using the same DFT functional (optB88-vdW). The results for the hydrogen storage capacities of Li-decorated borophene slit pores are plotted in the next figures as red solid lines, and those of graphene slit pores are plotted in black. Two isotherm curves are shown for each type of capacity, gravimetric and volumetric; they correspond to room temperature, $T = 298.15$ K, and to a low temperature of $T = 80.15$ K (most of the experiments of hydrogen storage on solid nanoporous materials at low temperatures have been performed at 77 K [4,48–50] and 80.15 K [51]). The width of the pores has been changed from 4 to 20 Å and the pressure from 0.1 and 25 MPa.

3.1. Dependence of the hydrogen storage capacities on pore width

Fig. 6 shows the calculated hydrogen storage capacities of Li-decorated borophene and graphene slit pores for the maximum value of the studied pressure, 25 MPa, and at the two considered temperatures, 80.15 K and 298.15 K. The g_c and v_c of both kinds of pores exhibit a similar dependence with the pore size: the curves have a maximum and decrease towards a constant value. The g_c of the slit pore tends towards a constant value that is twice the g_c of the corresponding single layer under the same conditions of pressure and temperature. On the other hand, the v_c decays to zero because the volume ratio $V_{\text{adsorbed}}/V_{\text{pore}}$ decreases as the pore width increases.

Although the variations of the hydrogen storage capacities of the Li-decorated borophene and graphene slit pores with the pore width have similar general features, important differences arise. Specifically, the maxima of the gravimetric and volumetric curves of Li-decorated borophene slit pores are located at pore widths smaller than those of the corresponding maxima of the graphene counterparts (see Table 2). On the other hand, the highest g_c at any temperature corresponds always to the graphene slit pore. However, the highest v_c at 80.15 K corresponds to the Li-decorated borophene slit pore, while at 298.15 K the result is in

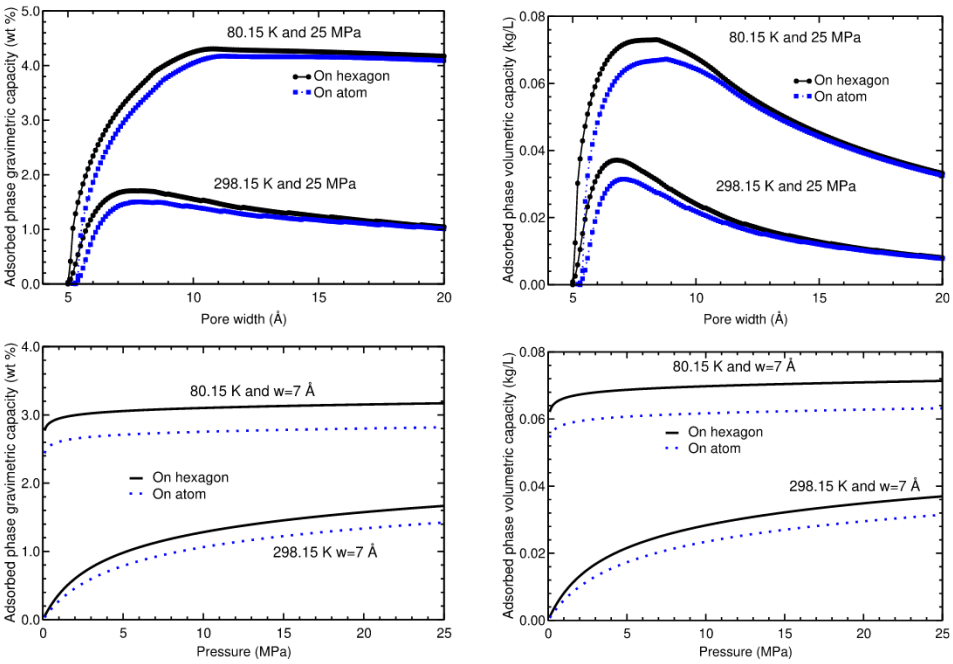

Fig. 5. Gravimetric and volumetric hydrogen storage capacities of graphene slit pores for 80.15 K and 298.15 K and two configurations, $H_{|||}$ and $A_{|||}$. Upper panel: Capacities as functions of the pore width, for a pressure of 25 MPa. Lower panel: Capacities as functions of the pressure, for a pore width of 7 Å.

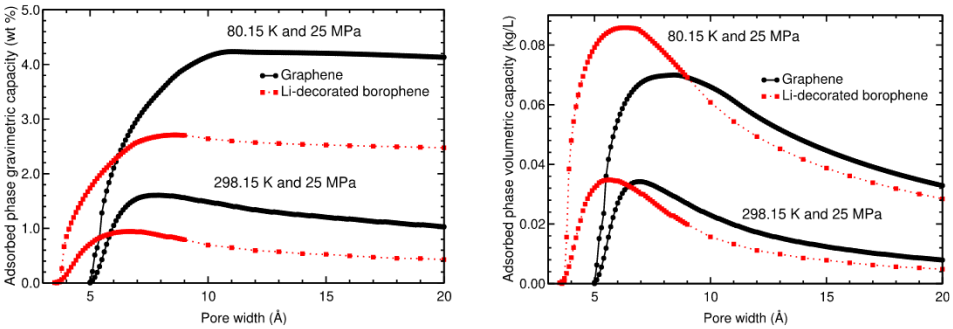

Fig. 6. Gravimetric and volumetric hydrogen storage capacities of slit pores of Li-decorated β borophene (red curves), as functions of the pore width, for 80.15 K and 298.15 K, and a pressure of 25 MPa. Capacities for graphene slit pores are also shown (black curves). (For interpretation of the references to color in this figure legend, the reader is referred to the web version of this article.)

Table 2
Maxima of the hydrogen storage capacities of Li-decorated borophene and graphene slit pores at 25 MPa, as functions of the pore width.

Slit pore	Capacity	80.15 K	298.15 K
Graphene	g_c	11.1 Å 4.23 wt %	7.9 Å 1.61 wt %
Graphene	ν_c	8.4 Å 0.0700 kg/L	7.0 Å 0.0342 kg/L
Borophene-Li	g_c	8.8 Å 2.70 wt %	6.8 Å 0.93 wt %
Borophene-Li	ν_c	6.4 Å 0.0835 kg/L	5.6 Å 0.0340 kg/L

favour of the graphene one (although in the latter case the differences are small: 0.0371 and 0.0340 kg/L for graphene and Li-decorated borophene slit pores, respectively; see Table 2).

An important result that can be noticed in Fig. 6 is that, at a given temperature, the hydrogen storage capacities of Li-decorated borophene slit pores are larger than those of graphene ones for narrow or very narrow pores. In fact, there are crossing points in that figure: for a pore width below a crossing point, the hydrogen storage capacity of the Li-decorated borophene slit pore is larger than the corresponding capacity of the graphene slit pore, and hence the former is more appropriate for hydrogen storage. The specific value of the crossing point depends on the temperature and the type of capacity, gravimetric or volumetric, as it is shown in Table 3. Above the crossing points, the situation is the opposite. It is also worth to point out that, below 5.4 Å, the volumetric capacity of Li-decorated borophene slit pores at room temperature (298.15 K) is even larger than that of graphene slit pores at a temperature such small as 80.15 K (this is a relevant result since the decrease of the temperature is a way to increase the hydrogen storage capacity of porous materials, in general). Although we are comparing different slit pores, this result reflects the good ability of narrow Li-decorated borophene slit pores for hydrogen storage. We note that nanoporous boron frameworks, containing many regions of borophene slit-shaped pores,

Table 3
Crossing points (slit pore widths) in Å of the hydrogen storage capacities of Li-decorated borophene and graphene slit pores at 25 MPa and for two temperatures, 80.15 and 298.15 K.

Capacity	80.15 K	298.15 K
g_c	6.1	5.9
ν_c	9.0	6.4

could perhaps be formed by using zeolite as a sacrificial template, just as zeolite-template carbons (ZTC) are formed [39], and these structures could be subsequently doped with Li atoms to obtain solid porous materials with good hydrogen storage capacities.

The large capacities of Li-decorated borophene slit pores of narrow widths can be explained by analyzing the potential $V(x,y,z)+V(x,y,d-z)$ confining the H_2 molecules for different pore widths d (see upper panel of Fig. 3). Fig. 7 shows this potential, $V(z)+V(d-z)$, at the deepest and shallowest regions in the xy plane for six pore widths: 5.2, 5.6, 6.4, 7, 12 and 20 Å. Results for graphene slit pores (obtained with the same optB88-vdW functional) are also shown. The confining potential (in the isotropic approximation) has a single deep minimum for narrow pores and two separated minima for larger pore widths, that become two independent potentials when the pore width is large. We note that the confining interaction potential of a Li-decorated borophene slit pore contains xy points or regions of different depths, and that the real influence of the whole interaction potential is some average between the two extreme cases considered, the deepest and the shallowest regions. The exact or real three-dimensional interaction potential of graphene slit pore also contains regions of different depths. However, we have showed before that the graphene slit pore potential in the isotropic approximation, $V_{slitpore}(z;d)$, is a good or reasonable approximation to the real three-dimensional potential.

The confining interaction potential at the deepest region of the Li-decorated borophene slit pore is much deeper than that of the graphene slit pore for the narrower pores of widths 5.2 and 5.6 Å (see Fig. 7). Accordingly, in that region Li-decorated borophene slit pores can store much more hydrogen than graphene slit pores. At many other regions of the xy plane (between the deepest and the shallowest regions), Li-decorated borophene slit pores of those widths will store also more hydrogen than graphene slit pores. Thus, one can understand that this is what will happen on average. This explains the larger hydrogen storage capacities of Li-decorated borophene slit pores of narrow widths, as obtained in our calculations (see Fig. 6). For pores of medium widths, 6.4 and 7.0 Å, the interaction potentials at the deepest regions of Li-decorated borophene slit pores are as deep as the interaction potentials of graphene slit pores (see Fig. 7). So, one can understand again, at least qualitatively, that for pores of these widths the two types of pores can store similar amounts of hydrogen. Finally, at larger pore widths, 12 and 20 Å, the interaction potential at the deepest region of the Li-decorated borophene slit pore is again deeper than the interaction potential of graphene slit pore. However, on average, the graphene potential attracts more hydrogen than the Li-decorated borophene potential for those larger pore widths.

We note that for pore widths above 7–8 Å, the volumetric capacities, v_c, of Li-decorated borophene and graphene slit pores are similar for the same P and T, but the gravimetric capacities, g_c, of graphene slit pores are about two times larger than those of Li-decorated borophene slit pores (see Fig. 6). This difference has its origin in the larger surface mass density of Li-decorated borophene with respect to that of graphene (6.75 u/Å^2 against 4.59 u/Å^2). This larger surface mass density implies that Li-decorated borophene slit pores have a larger mass of adsorbent material than graphene slit pores for a fixed pore volume. Hence, according to Eq. 7, if the mass of hydrogen (or equivalently the density of hydrogen and

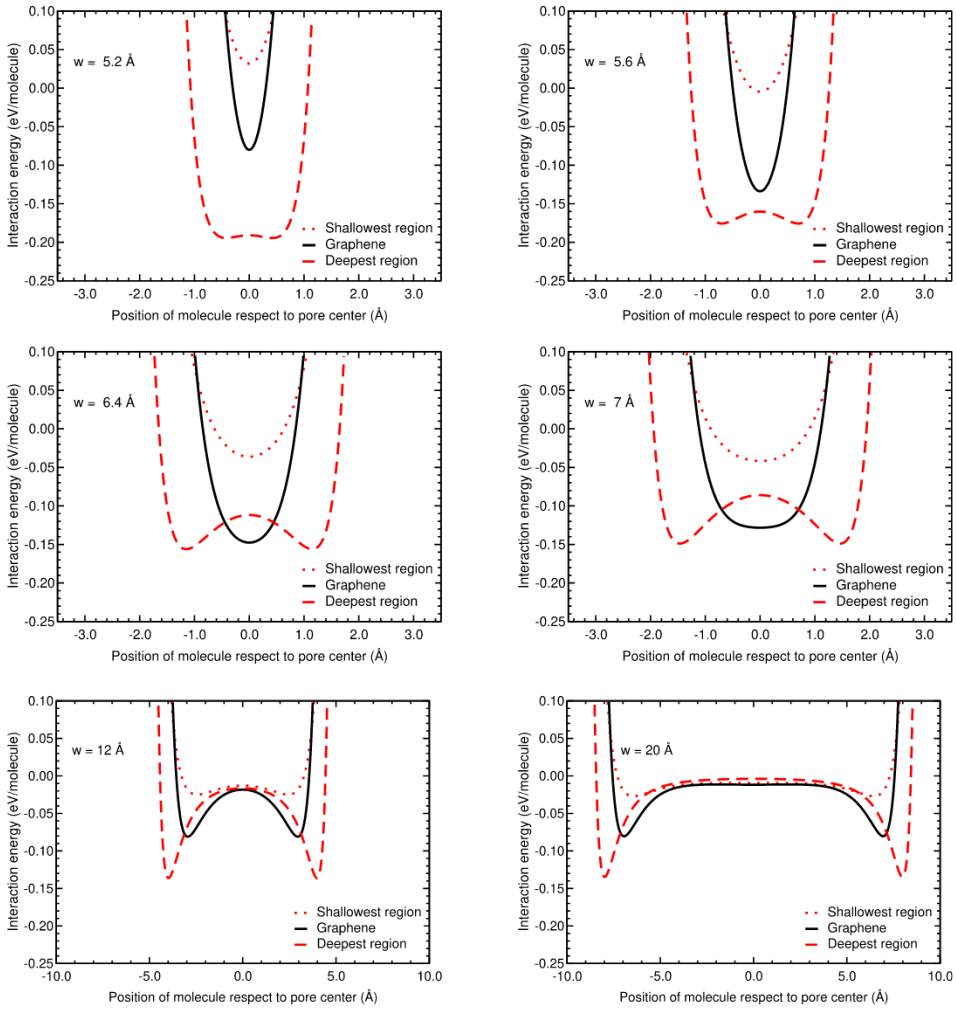

Fig. 7. Interaction potential $V_{slitpore}(z;d) = V(z)+V(d-z)$ confining the H_2 molecule in slit pores with six pore widths: 5.2, 5.6, 6.4, 7, 12 and 20 Å.

pore volume) is the same, Li-decorated borophene slit pores will have smaller g_c than graphene slit pores.

3.2. Dependence of the hydrogen storage capacities on the pressure

Fig. 8 shows the calculated g_c and v_c of Li-decorated borophene and graphene slit pores as functions of the pressure at a constant temperature (T = 80.15 or T = 298.15 K) for different pore widths. For a pore width of 7 Å (the width for which the v_c of the graphene slit pore at 298.15 K is maximum; see Table 2), the g_c is bigger for graphene slit pores at the two considered temperatures. Note that when the pressure decreases, the changes in the g_c are more important at room temperature, especially for the graphene slit pore below 10 MPa. The v_c of the pores of width 7 Å show similar features to those of the g_c at room temperature; however, at low temperature the behavior is quite different: the v_c of the Li-decorated borophene slit pore is bigger than that of the graphene slit pore for all studied pressures.

For a width of 6.4 Å (the width at which the v_c of the Li-decorated borophene slit pore is maximum at 80.15 K; see Table 2), the gravimetric and volumetric curves are similar to those obtained for the pores with a width of 7 Å. However, for a pore width of 5.6 Å (the width at which the Li-decorated borophene slit pore has the maximum v_c at room temperature; see Table 2), the behaviour changes drastically: the v_c and g_c of Li-decorated borophene slit pores become larger than those of graphene slit pores for any value of the pressure and temperature. It should be noted that, for this pore width, the v_c of Li-decorated borophene pores at 80.15 K are almost twice those of graphene slit pores. Finally, for pores of width 5.2 Å, the trends observed at the pore width of 5.6 Å are amplified: the capacities of Li-decorated borophene slit pore are larger and even much larger than those of the graphene slit pore at any value of the pressure and temperature. Above 4 MPa and for a pore width of 5.2 Å, the v_c of the Li-decorated borophene slit pore at 298.15 K

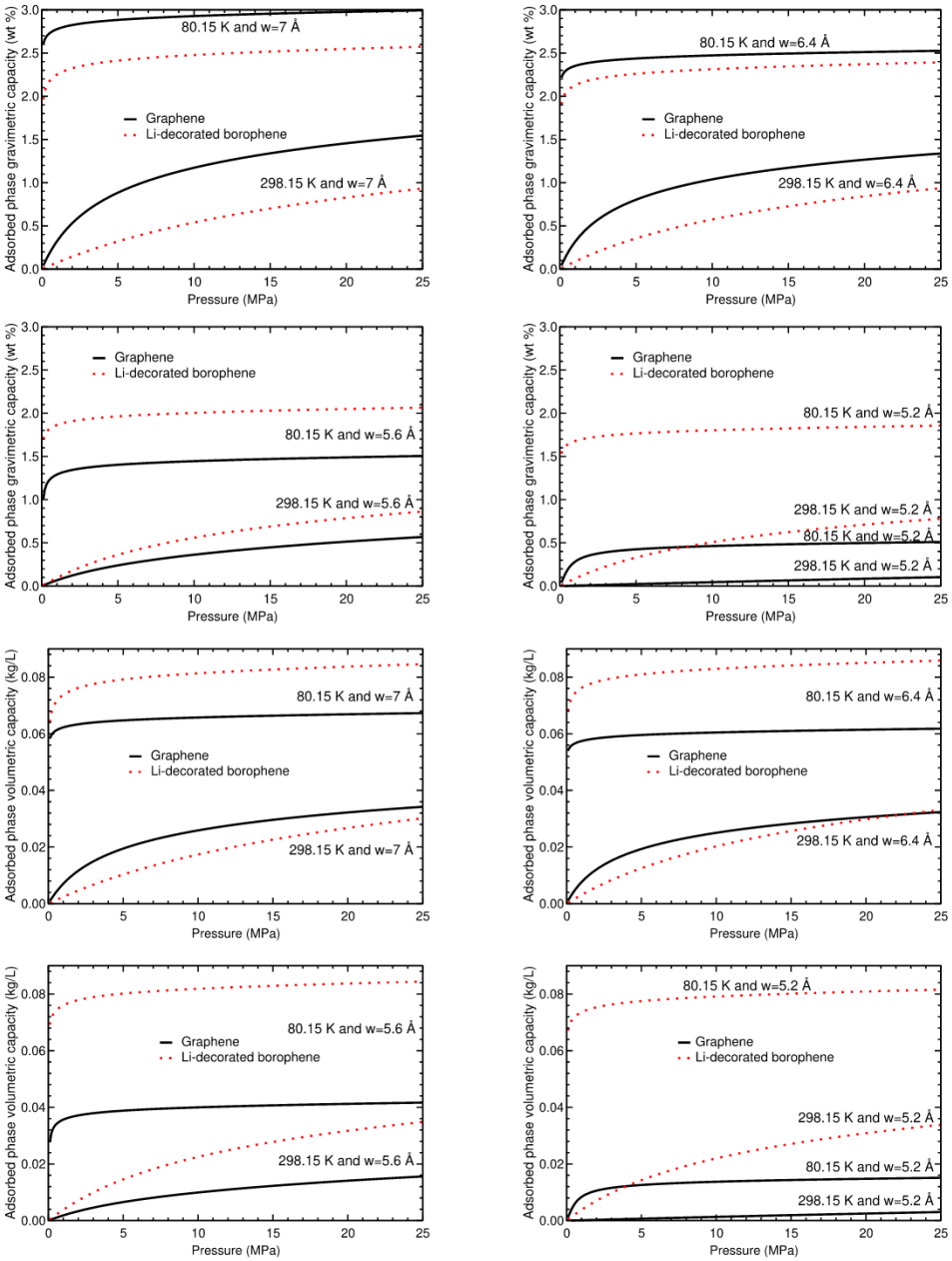

Fig. 8. Gravimetric (upper panels) and volumetric (lower panels) hydrogen storage capacities of the Li-decorated borophene slit pore (red curves), as a function of pressure, at 80.15 K and 298.15 K, for pore widths of 7, 6.4, 5.6 and 5.2 Å. Capacities of graphene slit pores are also shown (black curves). (For interpretation of the references to color in this figure legend, the reader is referred to the web version of this article.)

is even larger than that of the graphene slit pore at low temperature, 80.15 K.

4. Conclusions

In this work, we used a novel method that combines vdW-corrected DFT and a quantum-thermodynamic model to investigate in a realistic way the temperature and pressure dependencies of the hydrogen storage capacities of slit pores of Li-decorated sheets of borophene in its most stable Pmmn8 configuration. Thus, our results surpass the information provided in previous studies reporting the hydrogen storage capacity of Li-decorated borophene by means of standard DFT, only valid at zero temperature and no pressure [35–37]. Our results for Li-decorated borophene slit pores are compared with those obtained for graphene slit pores, which were previously investigated by some of us to analyze the effect of confinement on the hydrogen storage capacity of undoped carbon nanostructures [21,22].

The main result of our calculations is that narrow slit pores of the strongly anisotropic β (Pmmn8) Li-decorated borophene sheet have a good volumetric hydrogen storage capacity, especially at low temperature. The volumetric capacity of narrow Li-decorated borophene slit pores at room temperature is even larger than that of narrow graphene slit pores at low temperature, 80.15 K. Li-decorated borophene slit pores store hydrogen in very narrow pores, below pore widths of 5 Å, while the graphene slit pores do not store hydrogen in those very narrow pores.

The volumetric storage capacities at room temperature of Li-decorated borophene slit pores with pore widths in the range 5–6 Å are similar to the volumetric capacities at room temperature of graphene slit pores with larger pore widths, in the range 6–7 Å. At low temperature and for pore widths below 9 Å, the volumetric storage capacities of Li-decorated borophene slit pores are larger than the volumetric storage capacities of graphene slit pores.

We hope that these findings will stimulate the design of nanoporous boron frameworks, composed by many regions of borophene-like parallel surfaces, with optimal hydrogen storage capacities, particularly at low temperature. It is also worth to point out that, although our interest in the paper was mainly concerned with Li-decorated borophene slit pores, the new methodology proposed here can be useful for investigating the hydrogen storage capacity of other slit pores of anisotropic 2D materials doped with appropriate species.

CRediT authorship contribution statement

I. Cabria: Conceptualization, Formal analysis, Investigation, Methodology, Writing - original draft, Writing - review & editing. **A. Lebon:** Conceptualization, Formal analysis, Investigation, Methodology, Writing - original draft, Writing - review & editing. **M.B. Torres:** Conceptualization, Formal analysis, Investigation, Methodology, Writing - original draft, Writing - review & editing. **L.J. Gallego:** Conceptualization, Formal analysis, Investigation, Methodology, Writing - original draft, Writing - review & editing. **A. Vega:** Conceptualization, Formal analysis, Investigation, Methodology, Writing - original draft, Writing - review & editing.

Declaration of Competing Interest

The authors declare that they have no known competing financial interests or personal relationships that could have appeared to influence the work reported in this paper.

Acknowledgments

This research was financially supported by the Spanish MICINN (Grant PGC2018-093745-B-I00), the Junta de Castilla y León (Project No. VA124G18), the University of Valladolid, Spain, and the Xunta de Galicia (ED431E 2018/08, GRC ED431C 2016/001 and GRC ED431C 2020/10). We also acknowledge the use of the high performance computing equipment of the Pole de Calcul Intensif pour la Mer (DATARMOR, Brest) and the Centro de Proceso de Datos - Parque Científico (UVa).

References

[1] A. Kanygin, Y. Milrad, C. Thummala, K. Reifschneider, P. Baker, P. Marco, I. Yacoby, K.E. Redding, Rewiring photosynthesis: a photosystem I-hydrogenase chimera that makes H_2 in vivo, Energy Environ. Sci. 13 (2020) 2903–2914.
[2] P.S. Krishna, S. Styring, F. Mamedov, Photosystem ratio imbalance promotes direct sustainable H_2 production in Chlamydomonas reinhardtii, Green Chem. 21 (2019) 4683–4690.
[3] S. Rumpel, J.F. Siebel, C. Farès, J. Duan, E. Reijerse, T. Happe, W. Lubitz, M. Winkler, Enhancing hydrogen production of microalgae by redirecting electrons from photosystem I to hydrogenase, Energy Environ. Sci. 7 (2014) 3296–3301.
[4] D.P. Broom, C.J. Webb, G.S. Fanourgakis, G.E. Froudakis, P.N. Trikalitis, M. Hirscher, Concepts for improving hydrogen storage in nanoporous materials, Int. J. Hydrogen Energy 44 (2019) 7768–7779.
[5] M.D. Allendorf, Z. Hulvey, T. Gennett, A. Ahmed, T. Autrey, J. Camp, E.S. Cho, H. Furukawa, M. Haranczyk, M. Head-Gordon, S. Jeong, A. Karkamkar, D.-J. Liu, J. R. Long, K.R. Meihaus, I.H. Nayyar, R. Nazarov, D.J. Siegel, V. Stavila, J.J. Urban, S.P. Veccham, B.C. Wood, An assessment of strategies for the development of solid-state adsorbents for vehicular hydrogen storage, Energy Environ. Sci. 11 (2018) 2784–2812.
[6] C. Ahn, J. Purewal, Storage materials based on hydrogen physisorption, in: Hydrogen Storage Technology. Materials and Applications, CRC Press, 2016, pp. 213–238.
[7] D. Pukazhselvan, V. Kumar, S.K. Singh, High capacity hydrogen storage: Basic aspects, new developments and milestones, Nano Energy 1 (2012) 566–589.
[8] K.J. Gross, K.R. Carrington, S. Barcelo, A. Karkamkar, J. Purewal, P. Parrilla, Recommended best practices for the characterization of storage properties of hydrogen storage materials, Report to the Department of Energy Office of Energy Efficiency and Renewable Energy Hydrogen Storage Program under National Renewable Energy Laboratory Contract No. 147388, H2 Technology Consulting LLC (2012). http://energy.gov/eere/fuelcells/downloads/recommended-best-practices-characterization-storage-properties-hydrogen-0 and http://energy.gov/sites/prod/files/2014/03/f12/best_practices_hydrogen_storage.pdf (accessed October 16, 2020).
[9] D.P. Broom, Hydrogen sorption properties of materials, in: Hydrogen Storage Materials. The Characterisation of Their Storage Properties, Springer-Verlag, London, 2011, pp. 61–116.
[10] C. Liu, F. Li, L.-P. Ma, H.-M. Cheng, Advanced materials for energy storage, Adv. Mater. 22 (2010) E28–E62.
[11] L. Schlapbach, A. Züttel, Hydrogen storage materials for mobile applications, Nature (London) 414 (2001) 353–358.
[12] K. Kaneko, F. Rodríguez-Reinoso (Eds.), Nanoporous Materials for Gas Storage, Springer Singapore, New York, 2019.
[13] M. Hirscher, M. Becher, M. Haluska, F. von Zeppelin, X. Chen, U. Dettlaff-Weglikowska, S. Roth, Are carbon nanostructures an efficient hydrogen storage medium? J. Alloys Comp. 356 (2003) 433–437.
[14] J.S. Arellano, L.M. Molina, A. Rubio, J.A. Alonso, Density functional study of adsorption of molecular hydrogen on graphene layers, J. Chem. Phys. 112 (2000) 8114–8119.
[15] Office of Energy Efficiency & Renewable Energy, Fuel Cell Technologies Office, Materials-based hydrogen storage. https://www.energy.gov/eere/fuelcells/materials-based-hydrogen-storage (accessed October 16, 2020).
[16] Office of Energy Efficiency & Renewable Energy, Fuel Cell Technologies Office, DOE technical targets for onboard hydrogen storage for light-duty vehicles. https://www.energy.gov/eere/fuelcells/doe-technical-targets-onboard-hydrogen-storage-light-duty-vehicles (accessed October 16, 2020).
[17] S.K. Bhatia, A.L. Myers, Optimum conditions for adsorptive storage, Langmuir 22 (2006) 1688–1700.
[18] J. Li, T. Furuta, H. Goto, T. Ohashi, Y. Fujiwara, S. Yip, Theoretical evaluation of hydrogen storage capacity in pure carbon nanostructures, J. Chem. Phys. 119 (2003) 2376–2385.
[19] T. Yildirim, S. Ciraci, Titanium-decorated carbon nanotubes as a potential high-capacity hydrogen storage medium, Phys. Rev. Lett. 94 (2005) 175501.
[20] A. Lebon, J. Carrete, L.J. Gallego, A. Vega, Ti-decorated zigzag graphene nanoribbons for hydrogen storage. A van der Waals-corrected density-functional study, Int. J. Hydrogen Energy 40 (2015) 4960–4968.
[21] I. Cabria, M.J. López, J.A. Alonso, Simulation of the hydrogen storage in nanoporous carbons with different pore shapes, Int. J. Hydrogen Energy 36 (2011) 10748–10759.
[22] I. Cabria, M.J. López, J.A. Alonso, The optimum average nanopore size for hydrogen storage in carbon nanoporous materials, Carbon 45 (2007) 2649–2658.
[23] S. Patchkovskii, J.S. Tse, S.N. Yurchenko, L. Zhechkov, T. Heine, G. Seifert, Graphene nanostructures as tunable storage media for molecular hydrogen, Proc. Natl. Acad. Sci. U.S.A. 102 (2005) 10439–10444.
[24] F. Ersan, D. Kecik, V. Özçelik, Y. Kadioglu, O.U. Aktürk, E. Durgun, E. Aktürk, S. Ciraci, Two-dimensional pnictogens: A review of recent progresses and future research directions, Appl. Phys. Rev. 6 (2019) 021308.

[25] X. Li, L. Tao, C. Zefeng, H. Fang, X. Li, X. Wang, J.-B. Xu, H. Zhu, Graphene and related two-dimensional materials: Structure-property relationships for electronics and optoelectronics, Appl. Phys. Rev. 4 (2017) 021306.
[26] C. Tan, X. Cao, X.-J. Wu, Q. He, J. Yang, X. Zhang, J. Chen, W. Zhao, S. Han, G.-H. Nam, M. Sindoro, H. Zhang, Recent advances in ultrathin two-dimensional nanomaterials, Chem. Rev. 117 (2017) 6225–6331.
[27] Y. Zhang, A. Rubio, G.L. Lay, Emergent elemental two-dimensional materials beyond graphene, J. Phys. D: Appl. Phys. 50 (2017) 053004.
[28] A. Gupta, T. Sakthivel, S. Seal, Recent development in 2D materials beyond graphene, Prog. Mater. Sci. 73 (2015) 44–126.
[29] Z.-Q. Wang, T.-Y. Lü, H.-Q. Wang, Y.P. Feng, J.-C. Zheng, Review of borophene and its potential applications, Front. Phys. 14 (2019) 33403.
[30] A.J. Mannix, X.F. Zhou, B. Kiraly, J.D. Wood, D. Alducin, B.D. Myers, Synthesis of borophenes: anisotropic, two-dimensional boron polymorphs, Science 350 (2015) 1513–1516.
[31] H. Tang, S. Ismail-Beigi, Novel precursors for boron nanotubes: the competition of two-center and three-center bonding, Phys. Rev. Lett. 99 (2007) 115501–115504.
[32] X.F. Zhou, X. Dong, A.R. Oganov, Q. Zhu, Y. Tian, H.T. Wang, Semimetallic two-dimensional boron allotrope with massless Dirac fermions, Phys. Rev. Lett. 112 (2014) 085502–085504.
[33] J. Carrete, W. Li, L. Lindsay, D.A. Broido, L.J. Gallego, N. Mingo, Physically founded phonon dispersions of few-layer materials and the case of borophene, Mater. Res. Lett. 4 (2016) 204–211.
[34] A. García-Fuente, J. Carrete, A. Vega, L.J. Gallego, What will freestanding borophene nanoribbons look like? An analysis of their possible structures, magnetism and transport properties, Phys. Chem. Chem. Phys. 19 (2017) 1054.
[35] S. Er, G.A. de Wijs, G. Brocks, DFT study of planar boron sheets: a new template for hydrogen storage, J. Phys. Chem. C 113 (2009) 18962.
[36] L. Li, H. Zhang, X. Cheng, The high hydrogen storage capacities of Li-decorated borophene, Comput. Mater. Sci. 137 (2017) 119124.
[37] A. Lebon, R.H. Aguilera del Toro, L.J. Gallego, A. Vega, Li-decorated Pmmn8 phase of borophene for hydrogen storage. A van der Waals corrected density-functional study, Int. J. Hydrogen Energy 44 (2019) 1021.
[38] J. Klimeš, D.R. Bowler, A. Michaelides, Chemical accuracy for the van der Waals density functional, J. Phys.: Condens. Matter 22 (2010) 022201.
[39] H. Nishihara, T. Kyotani, Zeolite-templated carbons - three-dimensional microporous graphene frameworks, Chem. Commun. 54 (2018) 5648.
[40] G. Kresse, J. Furthmüller, Efficient iterative schemes for ab initio total-energy calculations using a plane-wave basis set, Phys. Rev. B 54 (1996) 11169–11186.
[41] G. Kresse, J. Hafner, Ab initio molecular dynamics for liquid metals, Phys. Rev. B 47 (1993) 558–561.
[42] P.E. Blöchl, Projector augmented-wave method, Phys. Rev. B 50 (1994) 17953–17979.
[43] M.-S. Park, S.-E. Lee, M.I. Kim, Y.-S. Lee, CO_2 adsorption characteristics of slit-pore shaped activated carbon prepared from cokes with high crystallinity, Carbon Lett. 16 (2015) 45–50.
[44] I. Cabria, Simulations of volumetric hydrogen storage capacities of nanoporous carbons: Effect of dispersion interactions as a function of pressure, temperature and pore width, Int. J. Hydrogen Energy 45 (2020) 5697–5709.
[45] A.F. Ismail, K.C. Khulbe, T. Matsuura, Gas Separation Membranes: Polymeric and Inorganic, Springer, Switzerland, 2015. doi: 10.1007/978-3-319-01095-3.
[46] R.C. Weast, Chemical Rubber Company, Handbook of Chemistry and Physics: A Ready-reference Book of Chemical and Physical Data, CRC handbook series, Chemical Rubber Company, 1972.
[47] I. Cabria, M.J. López, J.A. Alonso, Searching for DFT-based methods that include dispersion interactions to calculate the physisorption of H_2 on benzene and graphene, J. Chem. Phys. 146 (2017) 214104.
[48] R. Grünker, V. Bon, P. Müller, U. Stoeck, S. Krause, U. Mueller, I. Senkovska, S. Kaskel, A new metal-organic framework with ultra-high surface area, Chem. Commun. 50 (2014) 3450–3452.
[49] Y. Gogotsi, C. Portet, S. Osswald, J.M. Simmons, T. Yildirim, G. Laudisio, J. E. Fischer, Importance of pore size in high-pressure hydrogen storage by porous carbons, Int. J. Hydrogen Energy 34 (2009) 6314–6319.
[50] B. Schmitz, U. Müller, N. Trukhan, M. Schubert, G. Férey, M. Hirscher, Heat of adsorption for hydrogen in microporous high-surface-area materials, Comput. Phys. Commun. 9 (2008) 2181–2184.
[51] N. Ismail, Y.M. Temerk, A.A. El-Meligi, M.A. Badr, M. Madian, Synthesis and characterization of $MnPS_3$ for hydrogen sorption, J. Solid State Chem. 183 (2010) 984–987.